Journal of Biomedical Optics

BiomedicalOptics.SPIEDigitalLibrary.org

Morphology, topography, and optics of the orthokeratology cornea

Miguel Faria-Ribeiro
Rafael Navarro Belsue
Norberto López-Gil
José Manuel González-Méijome

SPIE.

Miguel Faria-Ribeiro, Rafael Navarro Belsue, Norberto López-Gil, José Manuel González-Méijome, "Morphology, topography, and optics of the orthokeratology cornea," *J. Biomed. Opt.* **21**(7), 075011 (2016), doi: 10.1117/1.JBO.21.7.075011.

Morphology, topography, and optics of the orthokeratology cornea

Miguel Faria-Ribeiro,[a,*] Rafael Navarro Belsue,[b] Norberto López-Gil,[c] and José Manuel González-Méijome[a]
[a]University of Minho, Clinical and Experimental Optometry Research Laboratory, Center of Physics, School of Sciences (Optometry), Campus de Gualtar, Braga 4710-057, Portugal
[b]Consejo Superior de Investigaciones Científicas and Universidad de Zaragoza, Instituto de Ciencia de Materiales de Aragón, Facultad de Ciencias, P. Cerbuna, 12, Zaragoza 50009, Spain
[c]Universidad of Murcia, Facultad de Óptica y Optometría, Edificio 35 (Campus de Espinardo), Murcia 30100, Spain

Abstract. The goal of this work was to objectively characterize the external morphology, topography, and optics of the cornea after orthokeratology (ortho-k). A number of 24 patients between the ages of 17 and 30 years (median = 24 years) were fitted with Corneal Refractive Therapy® contact lenses to correct myopia between −2.00 and −5.00 diopters (D) (median = −3.41 D). A classification algorithm was applied to conduct an automatic segmentation based on the mean local curvature. As a result, three zones (optical zone, transition zone, and peripheral zone) were delimited. Topographical analysis was provided through global and zonal fit to a general ellipsoid. Ray trace on partially customized eye models provided wave aberrations and retinal image quality. Monozone topographic description of the ortho-k cornea loses accuracy when compared with zonal description. Primary (C_4^0) and secondary (C_6^0) spherical aberration (SA) coefficients for a 5-mm pupil increased 3.68 and 19 times, respectively, after the treatments. The OZ area showed a strong correlation with C_4^0 ($r = -0.49$, $p < 0.05$) and a very strong correlation with C_6^0 ($r = 0.78$, $p < 0.01$). The OZ, as well as the TZ, areas did not correlate with baseline refraction. The increase in the eye's positive SA after ortho-k is the major factor responsible for the decreased retinal optical quality of the unaccommodated eye. [DOI: 10.1117/1.JBO.21.7.075011]

Keywords: orthokeratology; corneal refractive therapy; spherical aberration; ocular aberrations; accommodation; myopia; myopia control; contrast sensitivity function; accommodative lag.

Paper 160013RR received Jan. 7, 2016; accepted for publication Jun. 20, 2016; published online Jul. 19, 2016.

1 Introduction

Orthokeratology (ortho-k), also known as corneal refractive therapy (CRT), is a safe and effective modality to correct low-to-moderate myopia[1] by flattening the central cornea with the overnight application of reverse geometry rigid gas permeable contact lenses (CLs).[2] The corneal epithelium is reshaped by thinning in the central cornea and thickening in the midperiphery.[2] These anatomical changes have huge optical consequences. Besides the correction of central myopia and a small reduction in with-the-rule astigmatism,[3] as the pupil dilates the quality of vision deteriorates due to the significant increase in optical aberrations,[4,5] leading to complaints of photic phenomena,[6,7] as well as fluctuations in vision over the course of the day due to the temporary and reversible nature of the treatment.[8] Once the correct corneal shape is well-established, the visual performance of ortho-k patients will then rely on the centration, area, and power distribution of the central flattened zone [treatment zone or optical zone (OZ)] and the surrounding steepening zone [transition zone (TZ)]. Other authors have attempted to estimate the dimensions of the OZ and TZ by visual inspection of the differential topographic maps[9] or by using an arbitrary criterion for segmentation of the different new formed zones.[10]

Quantitative methods to estimate the optical characteristics of the postortho-k corneal surface will potentially be useful in determining the impact of lens design changes on the topographical and visual outcomes.[11] Furthermore, the objective characterization of the front corneal surface of the ortho-k cornea may allow us to better understand the impact of the ortho-k corneal optics on visual performance and may eventually allow the optimization of lens designs. Optimal designs could then be used to achieve corrections such as the regulation of myopia progression, by acting on the peripheral defocus[12] or presbyopia correction by improving the depth of field and/or the accommodative response of the eye.[13]

Thus, the first goal of the present work was to conduct an objective morphological, topographical and optical characterization of the ortho-k cornea using an algorithm of classification that analyzes the mean curvature from the post-treatment topographic map raw data. Subsequently, the influences of those changes in the optical quality were also investigated. Due to the interest in these three types of analysis, three complementary methods were implemented: (1) automatic determination and morphological analysis of the optical, transition, and peripheral zones; (2) global and zonal topographical analysis by fitting a general ellipsoid topographic model; and (3) ray tracing in partially customized eye models of the patients to study their optical performance.

Throughout this paper, the term morphology refers to structure and size changes of the limited zones of the anterior post-ortho-k cornea, i.e., external morphology.

*Address all correspondence to: Miguel Faria-Ribeiro, E-mail: mig.afr@gmail.com

1083-3668/2016/$25.00 © 2016 SPIE

2 Material and Methods

2.1 *Ortho-k Patients and Measurements*

Twenty-four patients, between the ages of 17 and 30 years (median = 24 years), were fitted with Corneal Refractive Therapy® (Paflucon D, Paragon CRT®) CLs, for a period of 146 to 411 days (median = 278 days) prior to data collection to correct myopia between −2.00 and −5.00 diopters (D) (median = −3.41 D) with refractive astigmatism below 2.00 D. Paragon CRT® dual axis was used in subjects with limbus-to-limbus corneal astigmatism to improve centration of the treatment. Trial lenses were derived from sliding table nomograms provided by the manufacturer, which have shown high levels of predictability in terms of first trial success.[14] If needed, during the first two follow-ups, some CL parameters were changed to obtain a full correction of the myopic refraction with a well-centered treatment. Fitting was evaluated according to the recommendations of the manufacturer regarding fluorescein pattern, topographical evaluation, and refractive and visual outcomes. All the enrolled subjects were able to achieve logMAR 0.0 visual acuity without any further compensation. All procedures were performed according to the Declaration of Helsinki. Approval for the study was obtained from the ethics committee of University of Minho School of Sciences.

2.2 *Local Mean Curvature Maps*

Left eye anterior elevation topography maps were obtained from all patients before and after the initiation of the ortho-k treatments using Medmont E300 corneal topographer (Medmont, Victoria, Australia), with pupil center determined by the topographer as reference. Considering the high repeatability of the Medmont topographer,[15] only one topography per patient was used to extract the anterior elevation data, provided that it scored higher than 99 out of 100 (higher score) by the instruments acquisition software. All patients attending the measurement visit were wearing the lenses overnight for at least three consecutive days. Topographies were measured within one to two hours after lens removal during the morning period. The raw elevation data of each patient was exported to MATLAB® and used to calculate the mean curvature (H), which is the average of the principal curvatures k_1 and k_2, defined as the maximum and minimum curvatures of each sampled point among all orientations. Mathematically, the mean curvature was computed for each corneal point according to its expression for functions with the form $Z = Z(x, y)$ so-called Monge Patch[16]

$$H = \frac{(1 + Z_y'^2)\ Z_{xx}'' - 2Z_x'Z_y'Z_{xy}'' + (1 + Z_x'^2)Z_{yy}''}{2\left(\sqrt{1 + Z_x'^2 + \ Z_y'^2}\right)^3}, \qquad (1)$$

where Z_x', Z_y', Z_{xx}'', and Z_{yy}'', are the first and second derivatives along the horizontal and vertical directions, and Z_{xy}'' is the crossed second derivative.

The mean curvature can be expressed in keratometric diopters $H_D = 1000 \times (1 - 1.3375) \times H$, by assuming 1.3375 for the refractive index of the cornea. Optically, H_D is the local spherical equivalent, which is especially appropriated for our purposes.[17,18]

2.3 *Zonal Segmentation*

To correct myopia, the central cornea is flattened to induce a reversible change on the epithelial thickness profile, and the paracentral annular zone, of about 1.5 to 2.0 mm in width, surrounding the treatment zone, steepens in a direct relationship with the amount of central flattening needed to correct the myopic refractive error.[9] It is then expected that a successful treatment will produce a smooth central area with an almost constant power, surrounded by a zone with abruptly increasing curvature. However, this will depend on the amount of correction and the curvature distribution of the anterior corneal surface before treatment. A third zone, corresponding to the most peripheral area of the cornea, will then be automatically defined by the limits of the steeper zone. The aim of the segmentation algorithm is to identify each of these three newly formed zones. To achieve this, a cluster segmentation algorithm was implemented in MATLAB® based on its native k-means function similar to the one described by González et al.[19] for laser assisted in situ keratomileusis (LASIK) treated corneas. This algorithm was programmed to conduct an automatic segmentation based on the mean local curvature at each point. The algorithm assumes that each of the three sets of points of the different zones has a normal distribution of curvatures. Hence, the global histogram will show a mixture of three Gaussians. The k-means algorithm splits these Gaussians, assigning every point of the histogram to one of the three, according to the normalized Euclidean distance between the point and the Gaussian center. The result of the segmentation is that each point in the topography is assigned to one of the three zones, each represented by a binary mask. The main problem that arises from this approach is that some points from the peripheral zone (PZ)—normally more flat—will be assigned to the OZ, due to their resemblance in curvature after the treatment. This can be easily solved by reassigning the OZ points that lay beyond the TZ to the PZ. The OZ and TZ diameter and center coordinates (x_0, y_0) can be obtained by least squares fitting the perimeter of the correspondent binary mask to a free orientated ellipse. Thus, coordinates x_0, y_0 of the center of the OZ represent decentrations of the ortho-k treatments with respect to the entrance pupil center.

In order to compute the mean curvature maps, the original Medmont topography elevation data given in polar coordinates grid (300 spokes going counter clockwise with the first at the horizontal 3 o'clock position and 32 rings) were interpolated and resampled to a 9-mm-square Cartesian coordinate grid. Points that lay outside the topographer's measurement area were set to zero. A fourth "no data" zone was included in the segmentation algorithm to allocate the points that fall out of the measurement area. This process provides a direct analysis of the morphological changes induced by the ortho-k treatments and allows for an independent topographic fit of each zone.

2.4 *General Ellipsoid Model Fit*

It is clear that topographies of real corneas do not match any ideal models such as spheres, ellipsoids, biconics, and so on, but rather they exhibit different irregularities and departures from these simple geometries.[20] In the case of ortho-k corneas, it is expected that this difference will be higher than in non-treated corneas. One of the problems that may arise from the fitting approaches used by most corneal topographers is that the entire shape of the ortho-k treated cornea may not be well

described by the conic model coefficients, leading to biased estimates especially of the conic constants (asphericities).

In our approach, topographic data was described in terms of horizontal and vertical principal apical radius of curvature R_x, R_y and conic constants Q_x, Q_y [oblate ellipse ($Q > 0$); sphere ($Q = 0$); prolate ellipse ($0 > Q > -1$); parabola ($Q = -1$); hyperbola ($Q < -1$)]. This was accomplished by fitting the elevation data in correspondence to each of the new formed zones, plus a global fit (monozone), to a general ellipsoid with three orthogonal axes and free position and orientation. A detailed description of the model and least-squares fit can be found elsewhere.[20] This model, as well as all subsequent computations, was implemented using MATLAB® (The MathWorks Inc., Natick, Massachusetts). The source codes are available under request to the corresponding author. Their use is permitted for academic purposes only.

2.5 *Wavefront Error*

Optical modeling was used to calculate aberrations of our subjects based on their anterior cornea topographic data. We assumed the same internal optics for all subjects, which enabled us to estimate the contributions of the ortho-k treatments in the optical performance. Two series of 24 semicustomized eye models were created in Zemax-EE numerical ray tracing software, based on the Navarro accommodative eye model,[21] with the front surface of the cornea replaced by the individual anterior elevation data of each patient (pre and postortho-k) obtained from Medmont raw data. Detailed methodology can be found elsewhere.[22] The vitreous length (VL) was adjusted to produce emmetropia, through maximization of the Visual Strehl calculated from the modulation transfer function (MTF)[23] (see Sec. 2.6), in the ortho-k eye models. The same VL value was used to model the corresponding preortho-k eyes. Into-the-eye ray trace was performed to calculate on-axis aberrations of the eye models for a 5-mm entrance pupil. The wavefronts, sampled in 512×512 matrices, were exported to MATLAB® for additional processing. Results were calculated for 555-nm wavelength and reported according to the Optical Society of America standards for reporting the optical aberrations of eyes.[24]

2.6 *Retinal Image Quality*

Although it is unknown which criterion the human eye actually uses for focusing and the ideal optimization method is yet to be determined, several metrics have been used to estimate refraction from wavefront data.[23,25,26] When higher-order aberrations are significant Cheng et al.[23] found that image plane quality metrics such as the Visual Strehl ratio computed in frequency domain (MTF method) (VSMTF) are less biased by the high levels of spherical aberration (SA). This metric takes into account that different frequencies respond differently to defocus, and neural sensitivity varies with frequency[27] in accordance to visual channel theory, which establishes that the visual pathway decomposes the input signal into frequency bands.[28]

The theoretical estimation of the retinal image quality (RIQ) in our model eyes was calculated from the following expression:

$$\mathrm{RIQ} = \mathrm{VSMTF} = \frac{\int_{-\infty}^{\infty}\int_{-\infty}^{\infty}\mathrm{CSF}_N(fx,fy)\cdot\mathrm{MTF}(fx,fy)\mathrm{dfx\,dfy}}{\int_{-\infty}^{\infty}\int_{-\infty}^{\infty}\mathrm{CSF}_N(fx,fy)\cdot\mathrm{MTF}_{\mathrm{DL}}(fx,fy)\mathrm{dfx\,dfy}}. \quad (2)$$

VSMTF is a normalized measure of image quality defined as the volume under the visually weighted MTF for an aberrated eye divided by the corresponding volume for an optically perfect eye (diffraction limited). CSF_N is the nominal neural contrast sensitivity function[29] and MTF is the one computed in the eye model. $\mathrm{MTF}_{\mathrm{DL}}$ is the diffraction limited MTF corresponding to the 5-mm pupil used here. This image quality metric provides a single value normalized between 0 and 1. This criterion was also used for the determination of the refractive state of pre and postortho-K eye models (VSMTF Rx), using a method previously described.[30] All eye models were assumed to be well corrected for a 5-mm pupil diameter. This was accomplished by subtracting the VSMTF Rx from the wavefronts before all calculations.

2.7 *Statistical Analysis*

In what follows, all data are reported as means and standard deviations unless otherwise stated. Statistically significant correlations were marked with * and ** for $p < 0.05$ and $p < 0.01$, respectively.

3 Results

The upper panels in Fig. 1 illustrate local spherical equivalent (mean curvature), and the lower panels show the results of the segmentation algorithm, for three different patients (a, b, and c). From these examples, it is clear that three independent and well delimited zones are formed after the ortho-k treatment is established, although with different power distributions.

The average results are summarized in Tables 1–4.

The morphological data show that the average OZ diameter is 3.53 mm. OZ is slightly decentered by an average of about a tenth of mm in the temporal and inferior directions, but the high standard deviation values suggest a marked intersubject variability. When considered as a single zone, the mean curvature of the cornea did not change significantly following ortho-k treatment (diff = −0.18 D; $p > 0.05$). This was due to the flattening of the central cornea corresponding to the OZ (−2.27 D) being counterbalanced by a significant steepening of the cornea corresponding to the TZ (+2.08 D). RMS ellipsoid fit error increases from 1.48 μm in the preortho-k cornea up to more than double that value (3.48 μm) for the postortho-k cornea, which suggests that after the treatment, the cornea can hardly be approximated by the ellipsoid model. This is the reason why the multizone model was implemented. The fitting errors improve quite dramatically when separate zones are considered instead of the monozone approach. In fact, the change in spherical equivalent refraction (calculated using the VSMTF criterion) due to the ortho-k treatments seems to agree rather well with the mean apical radius of curvature change within the OZ, but not when these changes were calculated from the monozone model fit (see Table 2 and Fig. 2). An opposite trend is observed when comparing the OZ versus the TZ. The decrease in mean curvature inside the OZ is followed by an increase in the TZ by a similar amount. Although the apical radii that describe the postortho-k corneal TZ are flatter, their correspondent Q values are much more positive, which indicates a greater steeping of the corneal curvature away from the apex.

Table 3 contains data of the optical and image quality parameters. Primary (C_4^0) and secondary (C_6^0) SA coefficients (5-mm pupil) increased by 3.68 and 19 times, respectively, after the treatments. This seems to be in agreement with the changes also seen in the ellipsoids conic constants passing from negative

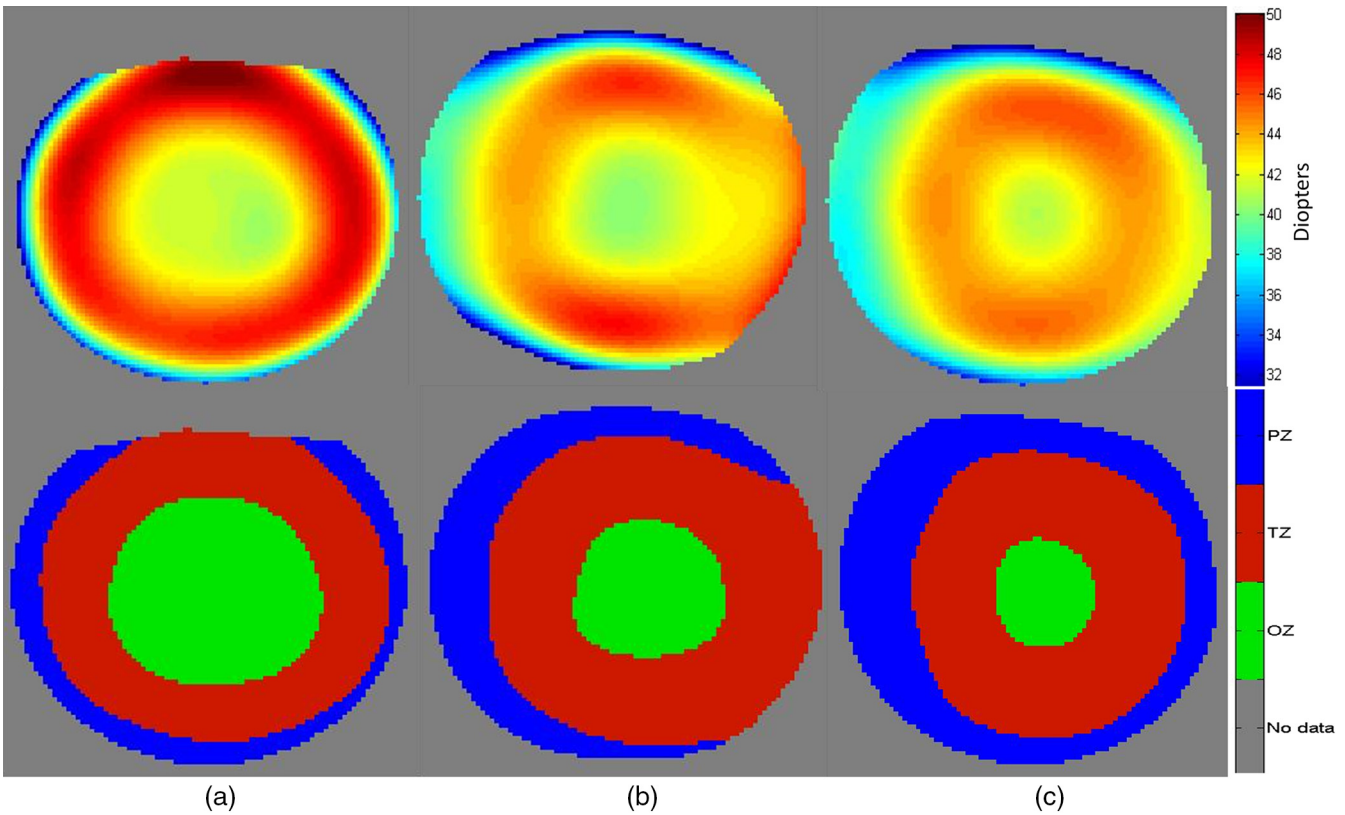

Fig. 1 Mean curvature maps of three distinct patients (a, b, and c) are shown in the upper panel. Examples of the resulting zonal segmentation obtained with the described algorithm are shown in the lower panel.

Table 1 Main topographical and morphological results (mean ± standard deviation) of the analysis of the ortho-k corneal topographies for the 24 subjects. RMSe represents the root-mean-square error that results from the least squares fit of the anterior cornea elevation data to an ellipsoid with three orthogonal axes. Length units are in mm, RMSe are in μm.

		Monozone		OZ		TZ	
		Pre	Post	Pre	Post	Pre	Post
				Morphologic data			
Diameter (mm)					3.53 ± 0.56		6.94 ± 0.25
Center (mm)	x_0				0.13 ± 0.25		0.08 ± 1.21
	y_0				-0.10 ± 0.20		0.00 ± 0.00
H_D (D)		42.3 ± 0.748	42.20 ± 0.72	43.93 ± 0.80	41.66 ± 0.73	42.98 ± 0.24	45.06 ± 0.24
				Topographic data			
R_X (mm)		7.68 ± 0.16	8.14 ± 0.19	7.71 ± 0.17	8.44 ± 0.21	7.69 ± 0.16	8.23 ± 0.18
R_Y (mm)		7.50 ± 0.15	7.91 ± 0.16	7.54 ± 0.15	8.26 ± 0.16	7.51 ± 0.15	8.03 ± 0.14
Q_X		-0.2 ± 0.067	0.40 ± 0.20	-0.16 ± 0.13	1.29 ± 0.70	-0.23 ± 0.08	0.71 ± 0.23
Q_Y		-0.2 ± 0.069	0.36 ± 0.19	-0.17 ± 0.13	1.24 ± 0.67	-0.25 ± 0.08	0.67 ± 0.22
RMSe (μm)		1.48 ± 0.47	3.48 ± 1.03	0.13 ± 0.08	0.22 ± 0.11	0.96 ± 0.38	1.36 ± 0.49

Table 2 Refractive changes (spherical equivalent) induced by the ortho-k treatments (mean ± standard deviation), calculated from different corneal descriptors. To convert from apical radius of curvature to diopters, a refractive index of 1.3375 was considered for the cornea.

Baseline SE	−3.71	±0.94	Pearson (r)
ΔRadius OZ	−3.83	±0.89	0.90**
ΔRadius Monozone	−2.40	±0.72	0.52*

Table 3 Main results (mean ± standard deviation) of the optical/image analysis of the ortho-k corneal topographies for the 24 subjects.

	Pre	Post
	Optical and image quality (5-mm pupil)	
C_4^0 (μm)	0.126 ± 0.03	0.464 ± 0.12
C_6^0 (μm)	0.001 ± 0.01	0.019 ± 0.03
C_3^1 (μm)	0.041 ± 0.11	−0.041 ± 0.29
C_3^{-1} (μm)	0.029 ± 0.15	0.069 ± 0.22
RIQ	0.32 ± 0.06	0.18 ± 0.06

to positive values (see Table 1). In addition, the small OZ average diameter means that peripheral rays pass through the more curved TZ, and hence these rays exhibit large amounts of positive SA. Horizontal third-order coma retains the same mean value but with the opposite sign, while the vertical component more than doubles, although still maintaining reasonably low values. Consequently, due to the high increase in SA, RIQ worsens—almost half VSMTF—in the ortho-k eye models compared to the pretreatment eyes. Although this does not seem to affect high-contrast visual acuity (all subjects achieved LogMAR 0.0), it is expected to deteriorate acuity for low-contrast tasks.

It is also expected that the changes in the anterior corneal shape after ortho-k produce changes in the optical performance of these eyes. To test this hypothesis, correlations between topographic, morphologic, and image quality descriptors were calculated and listed in Table 4. No adjustments for multiple comparisons were made, and such adjustments could potentially alter the significance of some of the correlations.

It can be seen that both horizontal and vertical coma correlate strongly with the OZ decentering (coordinates x_0 and y_0, respectively). The OZ area, as well as the difference between the OZ and TZ mean curvatures, showed a strong correlation with primary SA C_4^0 and a very strong correlation with secondary SA C_6^0. It seems that higher C_6^0 is associated with larger OZ's. As a consequence, RIQ showed a very strong-negative correlation with C_4^0 and a strong-positive correlation with C_6^0. The low correlation found between C_4^0 and the TZ area can be attributed to the use of a 5-mm entrance pupil, which will restrain part of the contribution of this zone to the image formation. The OZ, as well as the TZ, areas did not correlate with baseline spherical equivalent (PRE SE). As expected from the results in Table 1, the difference between the TZ and OZ mean curvatures (TZ–OZ) is strongly correlated with PRE SE, since the change in power tends to be redistributed between these two zones.

4 Discussion

The present study combines three complimentary methods of analysis of the morphology, topography, and optical/image quality of the postortho-k cornea. The first method and algorithm permits the objective quantification of the areas and power distribution across the different new formed zones—optical, transition, and peripheral zone. A similar methodology has been previously applied to the particular case of post-LASIK corneas by González el al.[19] The ortho-k treated cornea is a challenging condition as it usually includes significant asymmetries and irregularities. Lu et al.[9] delimitated the different zones using the difference curvature tangential map and used the size of the treatment zone as a metric to correlate with the visual outcomes during the treatment onset. While this approach could be sufficient for well-defined optic zones, it might become difficult and arbitrary in cases with narrow localized areas of flattening

Table 4 Pearson correlations between morphological, topographical, and RIQ descriptors for the postortho-k eye models. Only significant correlations are listed.

	Area		H_D	Q_{XY}		OZ			
	OZ	TZ	TZ—OZ	OZ	TZ	x_0	y_0	C_4^0	C_6^0
C_3^{-1}							−0.858**		
C_3^1						−0.936**			
C_4^0	−0.488*		0.588**	0.718**					−0.443*
C_6^0	0.780**	−0.464*	0.407*	−0.695**	0.456*			−0.443*	
RIQ	0.604**			−0.697**				−0.827**	0.576**
Pre-SE[a]			−0.764**	−0.590**		−0.414*		−0.836**	

[a]Preortho-k spherical equivalent error.
*$p < 0.01$.
**$p < 0.05$

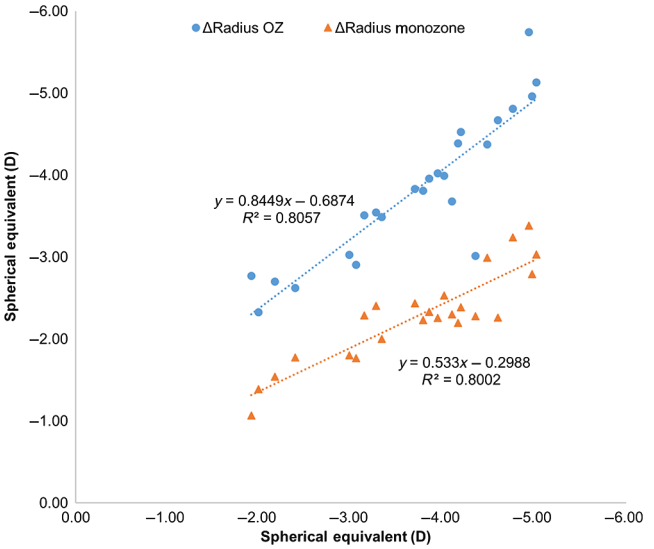

Fig. 2 Linear regressions of the results listed in Table 2. The slope of the linear regressions is indicative of the direct relation between refractive descriptors.

followed by wide areas of curvature change. Here, the mean curvature H was used instead, which has two crucial advantages. On the one hand, H is a physical invariant, which means that it is an intrinsic property of the corneal surface regardless of the measuring conditions. On the other hand, when multiplied by the increment of refractive index, it provides, in a first approximation, the local spherical equivalent.

For the topographical analysis, a general ellipsoid model[20] was implemented. It is worth mentioning that while the ellipsoid model provides reasonably good fits of normal corneas, the model fit gets poor in postortho-k corneas, similar to what happens in post-LASIK corneas.[19] Thus, elevation data fit to an ellipsoid by a monozone approach will not reflect the true shape of the ortho-k cornea. Instead, better fits are obtained when individual zones are fitted (see Table 1 RMS values monozone fit versus zonal fit), which implies that the increase in asphericity after ortho-k—especially in the OZ—would be largely underestimated by the monozone approach.

For the optical and image quality analysis, the pre and post-ortho-k wavefronts, computed by ray tracing on partially customized eye models, were compared. The strong-negative correlation between the OZ area and primary SA for a 5-mm pupil diameter seems to indicate that larger OZ's contribute to the decrease in positive C_4^0, but increase—with a more significant correlation—the contribution of positive C_6^0. Contrary to what one might expect, wide and well-defined OZ's were not correlated with lower baseline refractions. The lack of correlation between zonal areas and baseline refraction suggests that other factors rather than the degree of corneal remodeling—such as lid tonus and corneal biomechanics—play a more important role in the formation of those zones. It is worthwhile to remark that these resulting zones, OZ, TZ, and PZ, are defined according to the statistical distribution of the mean curvature descriptor, normalized for each analyzed cornea. This means that the resulting OZ is an area where the mean curvature has relatively homogeneous values, and the same applies to TZ and PZ.

Larger OZ's tend to have more homogeneous central zones with less-positive Q values ($r = -0.55$, $p < 0.01$). The central flattening creates a wider area of uniform power surrounded by a more peripheral steepening zone, as in Fig. 3(a), which increases the positive contribution of sixth-order SA ($C_6^0 > 0$) needed to fit the wavefront error profile. On the other hand, smaller OZ's, as in Fig. 3(c), tend to have smoother dioptric power changes from the center to the margin of the pupil with narrow and irregular zones of flattening, which decreases the positive contribution of sixth-order SA ($C_6^0 \leq 0$) needed to fit the wavefront error profile. The correlation found between C_4^0 and C_6^0 ($r = -0.44$; $p < 0.05$) results from the nature of Zernike polynomials, where higher-order polynomials include lower-order terms for balancing. Thus, considering the example of Fig. 3(a), the amount of C_4^0 needed to balance 0.06 μm of C_6^0 would be about 0.36 μm ($C_6^0 \times \sqrt{7/5} \times 5$), which indicates similar levels of Seidel primary and secondary SA. When considering the example of patient (c), the contrary is seen. The amount of C_4^0 needed to balance −0.03 μm of C_6^0 would be about −0.18 μm, which indicates a larger amount of primary Seidel SA.[31]

This increase in the eye's positive C_4^0 is the major factor responsible for the decrease in RIQ of the unaccommodated eye, estimated using the VSMTF metric, and might also influence its accommodative response.[32–35] It has been hypothesized that the increase in positive SA could provide an additional explanation for the myopia control effects obtained with different treatments in progressing myopes, due to a change in behavior of the accommodative system.[36–38] However, there is controversy in the results from different studies aiming to evaluate the actual changes in the accommodative system after

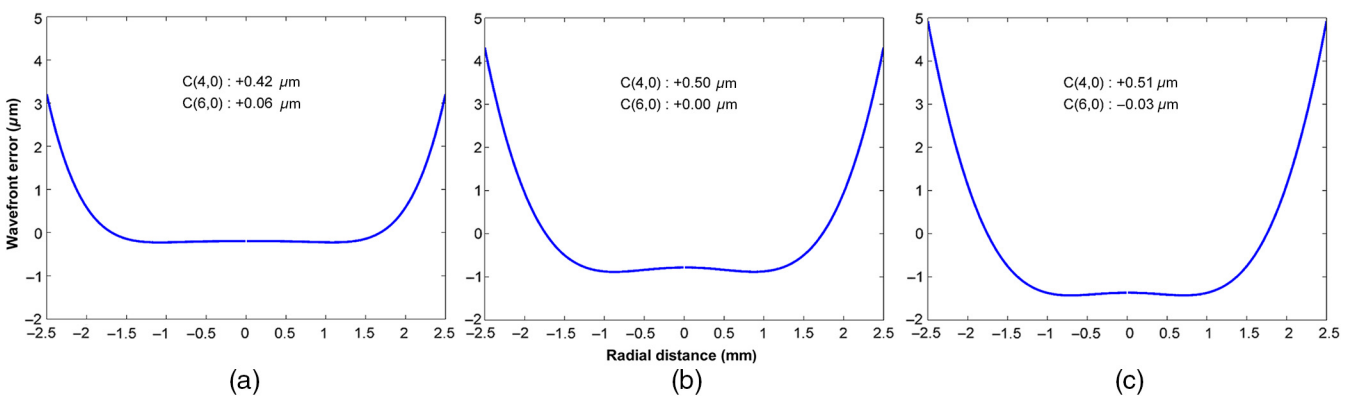

Fig. 3 Mean radial wavefront error profiles, representative of the optical path difference inside a 5-mm pupil after ortho-k, and their impact in C_4^0 and C_6^0, for the three eyes of Fig. 1 (patients a, b, and c).

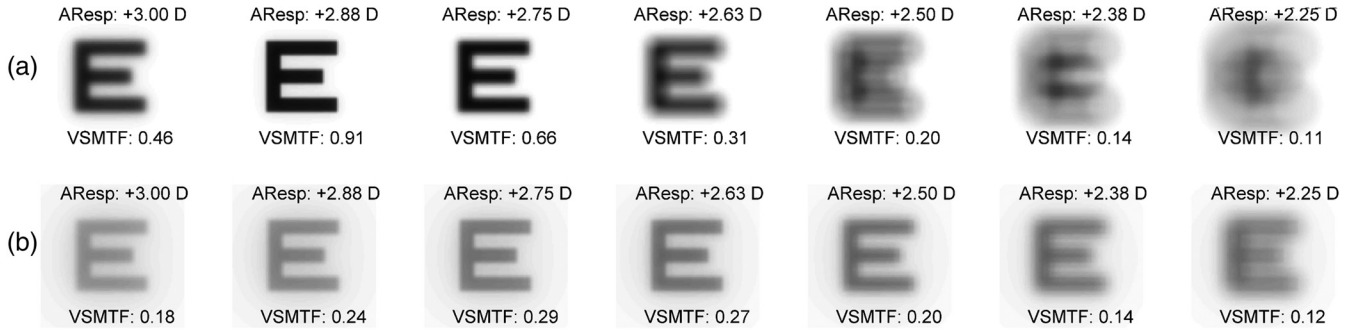

Fig. 4 Through-focus RIQ simulations for a 5-mm pupil, based on the Navarro accommodative eye model plus an SA phase plate to match the average SA values of our subjects before [(a) $C_4^0 = 0.126\ \mu$m; $C_6^0 = 0.001\ \mu$m] and after ortho-k [(b) $C_4^0 = 0.464\ \mu$m; $C_6^0 = 0.019\ \mu$m], for a −3.00 D TV. Pupil diameter decreases 0.35 mm/D of change in defocus with accommodation.

corneal reshaping with refractive surgery or ortho-k.[13,39,40] Gambra et al.[41] showed that adding negative fourth-order SA to an aberration-free eye produced a decrease in the accommodative lag, while adding positive fourth-order SA produced an increase in the accommodative lag (less-accurate accommodative response). A through-focus simulation was computed to illustrate this effect (see Fig. 4).

It appears that with the increase in positive SA after ortho-k, the eye will not need to accommodate as much for high-contrast resolution tasks such as reading. Judging from the through focus simulated retinal images of Fig. 4, the increase in positive SA provides a slight extension of depth of field (DoFi) when compared with the preortho-k simulations for a −3.00 D target vergence (TV). This seems to agree with experimental results, which showed that the presence of C_4^0 increases DoFi.[32,42,43] This observed causal relation might lead to two different results: on one hand, on a patient without accommodative lag, it is expected to decrease RIQ due to the loss of contrast induced by the high levels of positive SA; on the other hand, on a patient with accommodative lag—where acuity is compromised during near vision—the extended DoFi will increase retinal image resolution and therefore acuity for high-contrast tasks. Taking into account that the increment in positive C_4^0 after ortho-k presented a very strong-negative correlation with baseline myopia (Table 3; $r = -0.84$, $p < 0.01$), it is expected that this effect will be more beneficial in moderate myopes with decreased visual acuity at near, due to accommodative lag.

In summary, the present study provides a methodology to better understand the morphology, topography, and optics of the ortho-k cornea and their influence in the optical performance of these eyes. These conclusions might be useful to better understand the influences of ortho-k in myopia progression or to investigate future ortho-k lens designs to optimize the correction of refractive errors or presbyopia.

Acknowledgments

This work was funded in part by European Fund for Regional Development (FEDER) through the COMPETE Program and by the Portuguese Foundation for Science and Technology (FCT). FCT provided financial support in the framework of projects PTDC/SAU-BEB/098391/2008, PTDC/SAU-BEB/098392/2008 and the Strategic Project PEST-C/FIS/UI607/2011. The authors have no proprietary interest in the methods and devices described in this manuscript.

References

1. B. H. Koffler and J. J. Sears, "Myopia control in children through refractive therapy gas permeable contact lenses: is it for real?," *Am. J. Ophthalmol.* **156**, 1076–1081 (2013).
2. D. Z. Reinstein et al., "Epithelial, stromal, and corneal pachymetry changes during orthokeratology," *Optom. Vision Sci.* **86**, E1006–E1014 (2009).
3. J. Mountford and K. Pesudovs, "An analysis of the astigmatic changes induced by accelerated orthokeratology," *Clin. Exp. Optom.* **85**, 284–293 (2002).
4. A. Queirós et al., "Effect of pupil size on corneal aberrations before and after standard laser in situ keratomileusis, custom laser in situ keratomileusis, and corneal refractive therapy," *Am. J. Ophthalmol.* **150**, 97–109 (2010).
5. X. J. Mao, F. Lu, and J. Qu, "Effects after orthokeratology on corneal topography and monochromic wavefront aberration," *Zhonghua Yanke Zazhi* **40**, 471–473 (2004).
6. E. Santolaria et al., "Subjective satisfaction in long-term orthokeratology patients," *Eye Contact Lens Sci. Clin. Pract.* **39**, 388–393 (2013).
7. E. Santolaria Sanz et al., "Short-term changes in light distortion in orthokeratology subjects," *Biomed. Res. Int.* **2015**, 278425 (2015).
8. Y. Kobayashi et al., "Reversibility of effects of orthokeratology on visual acuity, refractive error, corneal topography, and contrast sensitivity," *Eye Contact Lens Sci. Clin. Pract.* **34**, 224–228 (2008).
9. F. Lu et al., "The relationship between the treatment zone diameter and visual, optical and subjective performance in corneal refractive therapy lens wearers," *Ophthalmic Physiol. Opt.* **27**, 568–578 (2007).
10. V. Maseedupally et al., "Central and paracentral corneal curvature changes during orthokeratology," *Optom. Vision Sci.* **90**, 1249–1258 (2013).
11. P. Kang, P. Gifford, and H. Swarbrick, "Can manipulation of orthokeratology lens parameters modify peripheral refraction?," *Optom. Vision Sci.* **90**, 1237–1248 (2013).
12. A. Queirós et al., "Peripheral refraction in myopic patients after orthokeratology," *Optom. Vision Sci.* **87**, 323–329 (2010).
13. G. Felipe-Marquez et al., "Accommodative changes produced in response to overnight orthokeratology," *Graefe's Arch. Clin. Exp. Ophthalmol.* **253**, 619–626 (2015).
14. M. López-López et al., "Contact lens intolerance: refitting with dual axis lens for corneal refractive therapy," *J. Optom.* **4**(1), 4–8 (2011).
15. P. Cho et al., "The performance of four different corneal topographers on normal human corneas and its impact on orthokeratology lens fitting," *Optom. Vision Sci.* **79**, 175–183 (2002).
16. A. Gray, "A Monge patch," in *Modern Differential Geometry of Curves and Surfaces With Mathematica*, 2nd ed., CRC Press, Boca Raton, FL (1997).
17. R. Navarro, "Refractive error sensing from wavefront slopes," *J. Vision* **10**, 3 (2010).
18. R. Navarro, "Objective refraction from aberrometry: theory," *J. Biomed. Opt.* **14**, 024021 (2009).

19. L. González, J. L. Hernández-Matamoros, and R. Navarro, "Multizone model for postsurgical corneas: analysis of standard and custom LASIK outcomes," *J. Biomed. Opt.* **13**, 044035 (2008).
20. R. Navarro, L. González, and J. L. Hernández, "Optics of the average normal cornea from general and canonical representations of its surface topography," *J. Opt. Soc. Am. A* **23**, 219–232 (2006).
21. R. Navarro, J. Santamaría, and J. Bescós, "Accommodation-dependent model of the human eye with aspherics," *J. Opt. Soc. Am. A* **2**, 1273–1281 (1985).
22. M. Faria-Ribeiro et al., "Computing retinal contour from optical biometry," *Optom. Vision Sci.* **91**, 430–436 (2014).
23. X. Cheng, A. Bradley, and L. N. Thibos, "Predicting subjective judgment of best focus with objective image quality metrics," *J. Vision* **4**, 310–321 (2004).
24. L. N. Thibos et al., "Standards for reporting the optical aberrations of eyes," *J. Refractive Surg.* **18**, S652–S660 (2002).
25. L. N. Thibos, "Unresolved issues in the prediction of subjective refraction from wavefront aberration maps," *J. Refractive Surg.* **20**, S533–S536 (2004).
26. L. N. Thibos et al., "Accuracy and precision of objective refraction from wavefront aberrations," *J. Vision* **4**, 329–351 (2004).
27. F. W. Campbell and J. G. Robson, "Application of Fourier analysis to the visibility of gratings," *J. Physiol.* **197**, 551–566 (1968).
28. M. B. Sachs, J. Nachmias, and J. G. Robson, "Spatial-frequency channels in human vision," *J. Opt. Soc. Am.* **61**, 1176–1186 (1971).
29. F. W. Campbell and D. G. Green, "Optical and retinal factors affecting visual resolution," *J. Physiol.* **181**, 576–593 (1965).
30. A. Guirao and D. R. Williams, "A method to predict refractive errors from wave aberration data," *Optom. Vision Sci.* **80**, 36–42 (2003).
31. R. Xu et al., "Modelling the effects of secondary spherical aberration on refractive error, image quality and depth of focus," *Ophthalmic Physiol. Opt.* **35**, 28–38 (2015).
32. Y. Benard, N. Lopez-Gil, and R. Legras, "Subjective depth of field in presence of 4th-order and 6th-order Zernike spherical aberration using adaptive optics technology," *J. Cataract Refractive Surg.* **36**, 2129–2138 (2010).
33. N. López-Gil and V. Fernández-Sánchez, "The change of spherical aberration during accommodation and its effect on the accommodation response," *J. Vision* **10**, 12 (2010).
34. N. López-Gil et al., "Retinal image quality during accommodation," *Ophthalmic. Physiol. Opt.* **33**, 497–507 (2013).
35. L. N. Thibos, A. Bradley, and N. López-Gil, "Modelling the impact of spherical aberration on accommodation," *Ophthalmic Physiol. Opt.* **33**, 482–496 (2013).
36. J. J. Walline et al., "Multifocal contact lens myopia control," *Optom. Vision Sci.* **90**, 1207–1214 (2013).
37. N. S. Anstice and J. R. Phillips, "Effect of dual-focus soft contact lens wear on axial myopia progression in children," *Ophthalmology* **118**, 1152–1161 (2011).
38. L. N. Thibos et al., "Spherical aberration and the sign of defocus," *Optom. Vision Sci.* **90**, 1284–1291 (2013).
39. F. Karimian et al., "Accommodative changes after photorefractive keratectomy in myopic eyes," *Optom. Vision Sci.* **87**, 833–838 (2010).
40. P. M. Allen et al., "Aberration control and vision training as an effective means of improving accommodation in individuals with myopia," *Invest. Ophthalmol. Vis. Sci.* **50**, 5120–5129 (2009).
41. E. Gambra et al., "Accommodative lag and fluctuations when optical aberrations are manipulated," *J. Vision* **9**(6), 1–15 (2009).
42. R. Legras, Y. Benard, and N. Lopez-Gil, "Effect of coma and spherical aberration on depth-of-focus measured using adaptive optics and computationally blurred images," *J. Cataract Refractive Surg.* **38**, 458–469 (2012).
43. K. M. Rocha et al., "Expanding depth of focus by modifying higher-order aberrations induced by an adaptive optics visual simulator," *J. Cataract Refractive Surg.* **35**, 1885–1892 (2009).

Miguel Faria-Ribeiro received his graduation degree in optics and optometry, his master's degree in advanced optometry, and his PhD in sciences-physiological optics from the University of Minho in 1999, 2011, and 2016, respectively. He has published 18 papers and 3 book chapters in the areas of myopia progression and visual control of eye growth, image quality, and CLs. He is a self-employed optometrist who collaborates with CEORLab.

Rafael Navarro Belsue received his PhD in physics from the University of Zaragoza in 1984. He is a professor of research at the National Council of Scientific Research. He was a visiting researcher at the Universities of Rochester and California, Berkeley. He is interested in physiological optics, vision, imaging, and image analysis. He has contributed more than 90 articles and more than 3000 citations (H-Index 29). He has directed 13 PhD theses and 23 R&D projects.

Norberto López-Gil received his master's degree in 1992, from University of Liège (Belgium), and PhD in 1997 from University of Valencia and worked as postdoctoral researcher from 1997 to 1998 (Cornell). Since 1999, he has been working as an associate professor in visual optics at the Universidad de Murcia. He has published about 60 articles and 120 presentations in scientific meetings and has 4 patents. Further details, see www.um.es/civium.

José Manuel González-Méijome received his graduation degree with honors in optics and optometry from the University of Santiago de Compostela in 1997 and his PhD in science from the University of Minho in 2007. Currently, he is an associate professor at the University of Minho and an Editor-in-Chief of the *Journal of Optometry–Peer Review Journal of the Spanish Council of Optometrists*. He has authored 135 articles indexed in ISI Web of Science with over 1500 citations, 3 books as main author, 15 book chapters, and 2 patent applications.